Original Article

Automatic segmentation and quantified analysis of meibomian glands from infrared images

Krishna Poojita Vunnava, Rohit Shetty, Sahana M Prabhu[1], Piyush Tiwari, Mathew Kurian Kummelil

Purpose: An algorithm for automated segmentation of meibomian glands from infrared images obtained using a novel prototype infrared hand-held imager has been proposed in this study. Meibomian gland dysfunction (MGD) is quantified in terms of five clinically relevant metrics. A comparison of these metrics in patients with MGD has been presented against a sample of the normative healthy population. **Methods:** This is a prospective cross-sectional observational study. Patients presenting to the clinics were enrolled after written informed consent. The everted eyelids of 200 eyes of patients (of which 100 were healthy and 100 were diagnosed with MGD) were imaged using a prototype hand-held camera. The proposed algorithm was used to process the images using enhancement techniques and the glands were automatically segmented. A comparison of glands of normal eyes versus MGD-affected eyes is performed using five metrics presented in this study: (i) drop-out, (ii) length, (iii) width, (iv) the number of glands, and (v) the number of tortuous glands. **Results:** The 95% confidence interval for the metrics did not show any overlap between the two groups. In MGD patients, the drop-out ratio was higher than normal. The length and number of glands were significantly lesser than normal. A number of tortuous glands were more in the MGD group. The metrics for MGD versus healthy and cut-off ranges were computed in the results. **Conclusion:** The prototype infrared hand-held meibographer and the proposed automatic algorithm for gland segmentation and quantification are effective aids in MGD diagnosis. We present a set of five metrics, which are clinically relevant for guiding clinicians in the diagnosis of MGD.

Key words: Automated analysis, dry eye disease, infrared meibography, meibomian gland dysfunction, normative data

Access this article online

Website: www.ijo.in

DOI: 10.4103/IJO.IJO_2930_22

Quick Response Code:

Meibomian gland dysfunction (MGD) is defined as a chronic, diffuse abnormality of the meibomian glands. This condition is characterized by terminal duct obstruction and/or qualitative and quantitative changes in glandular secretion.[1] The risk factors in the development of MGD include aging, contact lens use, and androgen deficiency.[2-4] High delivery and low delivery states of MGD have been described in the literature, of which the low delivery (obstructive) type is associated with sequential morphological changes of the glands.[1,5,6]

There is a lack of a single established objective criterion for the diagnosis of MGD.[7] Among the various modalities for *in-vivo* analysis of the morphology of meibomian glands, namely, optical coherence tomography (OCT), *in-vivo* confocal microscopy, and infrared systems, it is noted that infrared meibography is the most widely used.[8] Meibomian gland analysis based on infrared imaging has thus far relied upon gland drop-out ratio as the most widely used metric to classify MGD.[3,9-11] Various methods to grade the severity of MGD using imaging have been suggested in the literature, the most notable among them being the Pult scale[9] and the Meiboscale.[3,8,10,12,13] Such an analysis, based on a feature seen in the later stages of MGD, would result in missing out on early diagnosis and treatment. Various studies have shown a positive correlation between lid signs and meibum expression, with a drop-out ratio.[14] A few studies have analyzed morphological metrics such as drop-out ratio, irregularity, gland length, and width.[10,15,16] Meibograde scale considers gland distortion, the pattering of glands in its grading system.[16] However, none of them have compared the values of such metrics in normal and abnormal glands in various ethnic populations and none, particularly for Indian patients.

In this study, we have analyzed 200 eyes of equally distributed healthy and diseased patients, across various age groups in the Indian population. The proposed automated gland segmentation algorithm is detailed along with technical steps. We have computed an extensive set of five metrics based on gland morphology and presented the range of values for healthy versus MGD-affected patients, which is a helpful aid for speeding up the diagnosis by the doctors.

Methods

In this cross-sectional observational study, 200 eyes of patients who presented to the cataract, refractive, and dry

Department of Cataract and refractive surgery, Narayana Nethralaya, [1]Research and Technology Center, Robert Bosch Engg. and Business Solutions, Bangalore, India

Correspondence to: Dr. Krishna Poojita Vunnava, #501, Legend Apartments, Raj Bhavan Road, Hyderabad - 500 082, Telangana, India. E-mail: vkpoojita@gmail.com

Received: 03-Nov-2022 Revision: 29-Jan-2023
Accepted: 13-Feb-2023 Published: 05-Apr-2023

This is an open access journal, and articles are distributed under the terms of the Creative Commons Attribution-NonCommercial-ShareAlike 4.0 License, which allows others to remix, tweak, and build upon the work non-commercially, as long as appropriate credit is given and the new creations are licensed under the identical terms.

For reprints contact: WKHLRPMedknow_reprints@wolterskluwer.com

Cite this article as: Vunnava KP, Shetty R, Prabhu SM, Tiwari P, Kummelil MK. Automatic segmentation and quantified analysis of meibomian glands from infrared images. Indian J Ophthalmol 2023;71:1426-31.

eye clinics were imaged using a novel infrared hand-held imager (prototype). The study followed the tenets of the Declaration of Helsinki and the approval of the Institutional Review Board was taken. We considered patients between 15 and 70 years of age who were willing to undergo the scan (after valid informed consent). The group included those who were previously diagnosed with MGD, in addition to asymptomatic patients. The patients were categorized into MGD and normal groups based on slit-lamp findings of trained ophthalmologists. Patients who used contact lenses, those with a previous history of conjunctivitis of any etiology, corneal pathology, conjunctival and lid abnormalities, and images with poor quality were all excluded from the study.[3,17-19]

Meibography of the everted upper eyelid was performed using a hand-held imager (prototype) [Fig. 1(a)]. It is fitted with an infrared camera with a resolution of 5 MP, which has auto and manual modes of focus. We have imaged and analyzed only the upper eyelids, as they have a wider area of glands for studying morphology. After everting the lid, a single trained ophthalmologist acquired images in the autofocus mode. An example of the image taken by the device is presented in Fig. 1(b). In addition to the camera, the quality of the acquired image depends on several factors: (i) motion blur due to hand tremor or defocus blur due to improper focusing, (ii) insufficient eyelid exposure, (iii) uncooperative patient, and (iv) light reflections from the environment in the examination room. We subsequently enhanced the images using contrast-limited adaptive histogram equalization (CLAHE) [Fig. 1 (c)] and then subjectively evaluated the quality of these images. Poor-quality images and those with inadequate exposure leading to an erroneously small region of interest were excluded from this study.

We have developed an automatic software algorithm to analyze these images obtained from the hand-held imaging device. We have detailed the steps in the algorithm as follows. Please refer to Figs. 1 and 2 for the sequence of outputs at each stage of the algorithm:

1. The original image [Fig. 1 (b)] from the infrared camera [Fig. 1 (a)], and the enhanced image using CLAHE after post-processing [Fig. 1 (c)] are shown in Fig. 1. Note that the glands become visible to the observer after applying this enhancement alone, which shows that the hand-held imager can indeed capture good-quality images that are useful for analysis.
2. The next step in the algorithm is to check for any specular reflection artifacts (by applying thresholding) and replace those regions with mean values.
3. Noise reduction in the images was performed by applying a low-pass smoothening filter called the Butterworth filter.
4. Morphological operations that include dilation and erosion were also applied for the binarization of glands [Fig. 1(d)] so that the edges of the gland regions are emphasized.
5. Automatic segmentation of the glands was performed using the Gabor filter,[20] which is a wavelet-based filter that is suitable for the extraction of local textural features [Fig. 1(e)]. For this 2-D filter, we empirically selected the following parameters: (i) the number of scales = 5 (by considering zooming factors), (ii) the number of orientations = 20 (to correct for the possible tilt of the camera), (iii) spatial size of the filter window was fixed at (45,45). The result of Gabor filtering was then binarized at two different thresholds 119 and 135 for computing the metrics. It was observed that the higher threshold was more accurate while computing the length and drop-out, whereas the lower threshold was useful for computing the rest of the metrics: the number of glands, tortuosity, and width. Region of interest (ROI) was marked in the form of a hexagon manually by a trained ophthalmologist using the six landmark points and ensuring maximum coverage of the lid [Fig. 3]. Two points on the upper lid margin, two on the lower edge of the everted lid, and one each on the tapering edge at the corners. Note that

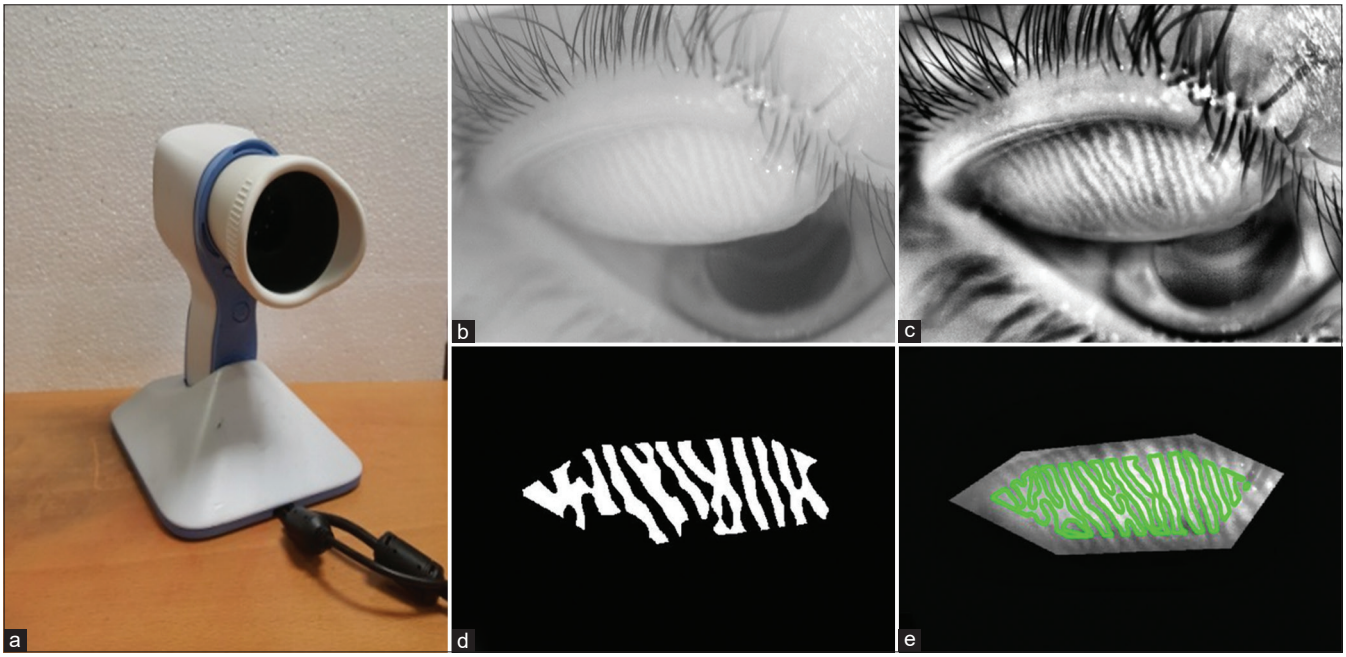

Figure 1: (a) Prototype device. (b) Image captured by prototype device. (c) Enhanced image. (d) Segmentation map. (e) Overlay on the image.

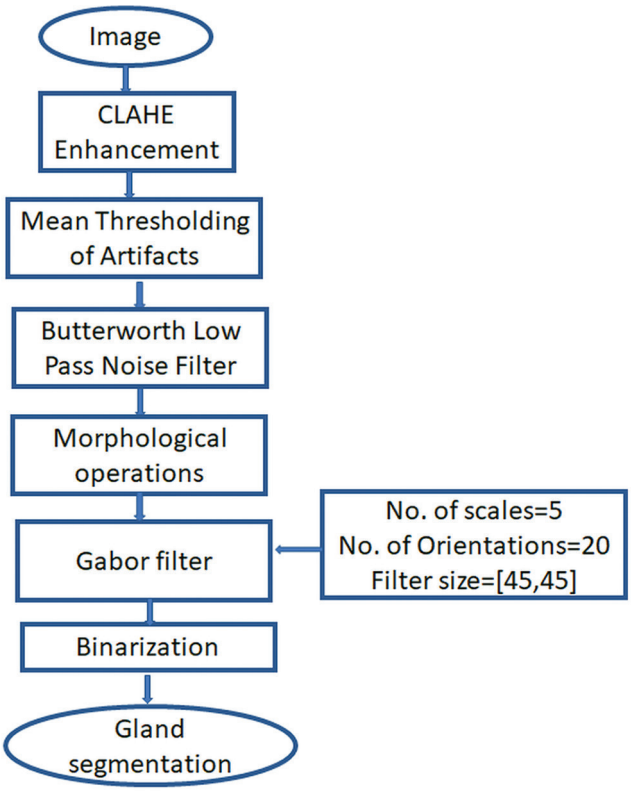

Figure 2: Depiction of the steps of the algorithm

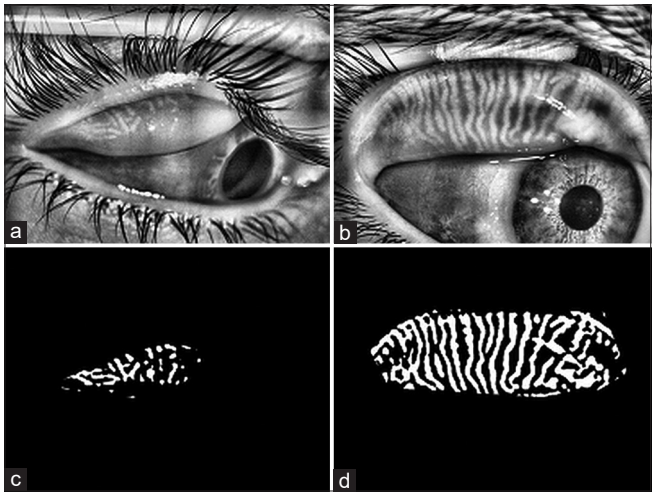

Figure 4: (a) Enhanced image of the upper lid showing significant dropouts. (b) Enhanced image of the upper lid showing an abundance of glands and a few shortened glands. (c) The segmentation map of the glands in the upper eyelid is shown in figure (a). (d) A segmentation map of the glands in the upper lid is shown in figure (b)

the ROI is only necessary for the computation of gland drop-out, and the other metrics are independent of the ROI. Two additional examples of diseased eyelids and their respective automatic gland segmentation outputs are shown in [Fig. 4a-d].

We have computed the following metrics for the quantitative assessment of the meibomian glands in each image.

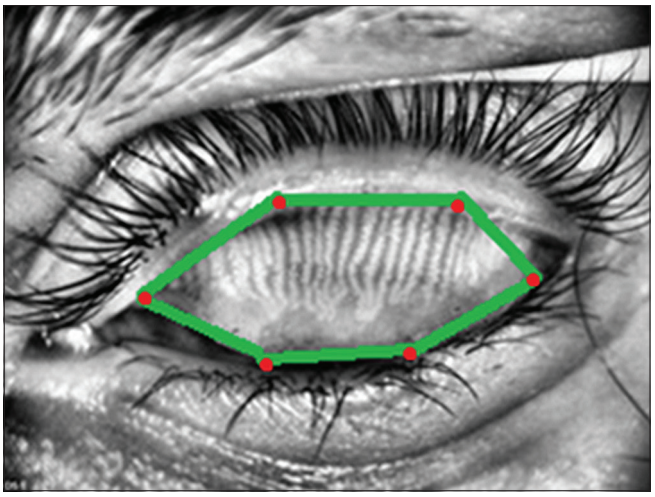

Figure 3: The region of interest is marked with six points (indicated in red) and the hexagonal polygon is filled from these points using the spline algorithm

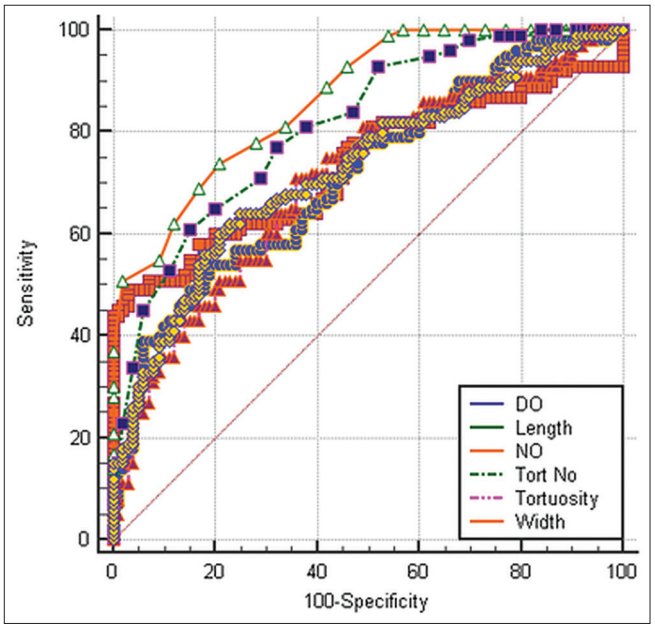

Figure 5: Receiver operating characteristic (ROC) curve plotted for five metrics denoting the highest area under the curve (AUC) for the number of tortuous glands and the width of the glands

(i) Gland drop-out (DO): Ratio of eyelid area that is not covered by glands to the total area of the eyelid considered in the ROI. This is a measure of the coverage of the glands in the eyelid and is the most used metric for MGD. Ghost glands were also considered dropouts. However, this shows a significant difference only for more advanced stages of the disease and is not apparent in the early stages.

(ii) Tortuosity and number of tortuous glands: Tortuosity measures the curvature of the gland, which is the ratio of the arc length of each gland to the distance between the endpoints of the gland. If this value is greater than a threshold of 1.2 (which we have determined based on our study of normal glands), then that gland is counted as tortuous.

(iii) Length: The distance (in pixels) when traversing along the skeletonized component of each of the glands is taken as the length. The average of the lengths of all the glands in each image is considered as a metric. In the clinical context, this length is computed from the upper edge seen at the mucocutaneous border to the lower blind end of the glands.

(iv) Width: We computed the median width (in pixels) of the glands at the mid-line of the image.

(v) Total number of glands (NO): This is the number of connected components in the binary mask of the automatically segmented glands. The automated markings were repeated thrice in a set of 10 eyes in diseased and normal groups to check the repeatability of the algorithm in detecting the glands. The metrics that were computed were compared between the two groups.

The automated markings were repeated thrice in a set of 10 eyes in diseased and normal groups to check the repeatability of the algorithm in detecting the glands. The metrics that were computed were compared between the two groups.

The repeatability of the measurements was studied using interclass correlation coefficient (ICC) obtained from three readings using the MedCalc software: 95% confidence interval (CI) computation, mean ± standard deviation (SD) was computed in the normal and diseased population using the SPSS software. Shapiro–Wilk test was used to test normality. The independent sample *t*-test was used to compare the healthy and diseased population in normally distributed samples and Mann–Whitney *U*-test was used for non-parametric data. The receiver operating characteristic (ROC) curve was plotted using the MedCalc software, and the Youden index (J value), sensitivity, and specificity values were derived for each metric.

Results

Of the 200 eyes analyzed, 120 belonged to females and 80 to males. The distribution across ages was kept uniform with 66 with age >50 years and the rest with age ≤50 years.[12]

ICC was used to study the repeatability of the algorithm in computing length, tortuosity, and drop-out in healthy and diseased showed a correlation coefficient of unity. Ninety-five percent CI values for each metric in the healthy and diseased population are mentioned in Table 1. The mean ± SD for the number of glands, number of tortuous glands, length, and width did not show any overlap and had a clear statistical difference of $P < 0.001$ between the two groups. The width of the gland showed a statistically significant difference; however, the range between the groups was close. The complete

Table 1: Metrics computed in the healthy and diseased subgroups

	Healthy	Diseased	*P* (Mann–Whitney *U*)
Number of glands			
95% CI*	23.88-26-64	14.63-16.75	<0.001
Mean±SD†	25.26±6.93	15.69±5.36	
Tortuosity			
95% CI	1.42-1.49	1.31-1.37	<0.001
Mean±SD	1.45±0.19	1.34±0.15	
Number of tortuous glands			
95% CI	13.60-16.14	7.16-8.90	<0.001
Mean±SD	14.87±6.38	8.03±4.37	
Length (Pixels)			
95% CI	186.06-213.52	149.19-167.64	<0.001
Mean±SD	199.79±69.17	158.41±46.50	
Width (Pixels)			
95% CI	15.29-16.04	13.61-14.43	<0.001
Mean±SD	15.66±1.87	14.02±2.05	
Drop out (Percentage)			
95% CI	53.25-55.89	60.78-65.65	<0.001
Mean±SD	54.42±5.88	63.22±12.27	

*CI- Confidence interval. †SD- Standard Deviation

Table 2: Statistical measure of the cut-off value for the five metrics

	Number of glands	Number of tortuous glands	Length (Pixel)	Width (Pixel)	Drop out (Percentage)
AUC*	0.86	0.81	0.71	0.72	0.73
J index†	0.53	0.46	0.35	0.39	0.46
Criterion	<19	>8	<157	14.21	>64
Sensitivity	74	61	54	60	49
Specificity	79	85	81	79	93

*Area under the curve. †Youden index

workflow of automatic gland segmentation demonstrating the order of the consecutive steps is presented [Fig. 2]. Youden's index for each metric was calculated to determine the optimal cut-off. It was calculated using the MedCalc software using the formula J = sensitivity + specificity − 1. The ROC for the metrics [Fig. 5], which was used to determine the diagnostic cut-offs (by circumventing the arbitrariness of diagnosis) while classifying the glands into normal and abnormal has been tabulated. Table 2 presents the area under the curve (AUC), Youden's index (J), the cut-off criterion for each metric, and sensitivity–specificity for each metric for that cut-off value [Fig. 5].

Discussion

The tear film and an ocular surface committee have defined MGD as a chronic, diffuse abnormality of the meibomian glands, characterized by terminal duct obstruction and/or qualitative/quantitative changes in the glandular secretion.[1] Two types of MGD have been described in the literature. An obstructive type of MGD is associated with hyper-keratinization and gland obstruction, which, in turn, leads to various morphological changes in the gland.[5,21] An International workshop report on anatomy and pathophysiology has described these sequential changes, which begin with dilation of the gland/duct secondary to obstruction, followed by tortuosity associated with stasis of secretions within the gland.[21,22] Persistence of obstruction beyond this stage leads to shortening of the glands and dropouts.[21] Hence, measurement of these morphological features and determining a normative range would be useful to monitor sequential changes. Studies have shown that lower lid morphology correlates with that in the upper lid.[23] Therefore, due to the consistency in the exposure of the glands and the wider area available, we preferred to evaluate the upper lid.

So far, most studies, which have analyzed MGD using meibography, have focused mainly on computing drop-out in the glands as a measure of severity. Meiboscore described by Arita *et al*. grades MGD by calculating the percentage of dropout of the glands in the lid.[10,13] Pult *et al*. defined a newer five-scale grading system, which focuses on sequential drop-out, albeit in smaller steps.[9] Drop-out occurs in the final stage of MGD and various treatment modalities such as warm compress, and thermal pulsation therapy, are of no significant benefit after the atrophy of glands. We measured the percentage of lid area without the glands (including the area between the glands). Reduction in the number of glands and thinning also contributed to an increase in this value. Hence, we believe that number of glands and width could be a better indicator of MGD than drop-out calculated in other studies. The gland drop-out was 54.42 ± 5.88% in healthy and 63.22 ± 12.27% in diseased with a statistically significant difference between the groups (P = 0.005). The AUC and Youden's index calculation showed that the criteria for cut-off for drop-out percentage in our study are >64% for a specificity of 85%. Yumiko *et al*.[24] have described gland length and dropouts in their study on 37 healthy adults. In a study by Quintana *et al*.,[15] the inter-reader variability in a subjective analysis of agreement for the meibomian gland was seen and a few metrics such as irregularity and length were computed. In our study, the mean length in the healthy eyes was 199.79 ± 69.17 pixels, whereas in the diseased eyes was 158.41 ± 46.50 pixels. The empirical cut-off which provides good sensitivity and specificity was <157 pixels.

Pathophysiologic analysis of obstructive MGD shows that after obstruction secondary to hyperkeratinization, the gland secretions undergo stasis distal to it and there is an increase in tortuosity and width of the glands. The number of tortuous glands would thus be an indicator of an earlier stage of the disease.

Pult *et al*.[23] have studied the bent angle of the worst gland to study tortuosity, assuming that it is an indicator of the health of overall glands. Machalinska *et al*.[14] have divided the groups based on the presence or absence of tortuous glands. We have calculated the ratio of the arc length of each gland to the total length and calculated the mean number of tortuous glands for the eye in the two groups. Glands have been considered tortuous when this ratio was more than 1.20 pixels. We have found a significant difference between normal and abnormal (P < 0.005) with an AUC of 0.81, where a value of more than eight indicates a diseased condition. However, we have noticed that the accuracy of gland detection in cases with highly tortuous glands depends on the quality of the image procured by the device. Machalinska *et al*.[14] have demonstrated that lid tortuosity did not correlate with meibomian gland loss and had a strong correlation with contact lens use and allergic conjunctivitis. However, they have not correlated the presence of tortuous glands with any clinical parameter. Given that number of tortuous glands was one of the more reliable markers of MGD in our study and patients with allergic conjunctivitis and contact lens users were excluded, we feel it is imperative to do imaging in addition to the clinical analysis of lid signs and meibum expressivity. We found that the total number of glands had the best diagnostic potential in terms of maximum AUC. The cut-off of < 18 glands had a specificity of 83. Pult *et al*. found that inter-observer and intra-observer agreement was better in objective grading (rather than subjective grading). Hence, an algorithm-based automated analysis of glands with a cut-off for normal and abnormal would have wider clinical utility.[9]

There are a few limitations in our study, which we describe here. We have classified the eyes as healthy based on the absence of signs on slit-lamp examination and morphological features. The inclusion of clinical features also introduces inter-observer variability and bias and classification based on imaging currently does not have a single standardized criterion. The width of the gland could be a very sensitive tool in the diagnosis of MGD. We calculated the width at a single plane; however, the measurement at multiple levels could possibly detect more subtle changes. Correlation with clinical features such as the quality of meibum can probably replace clinical methods with more objective analysis using imaging. Analysis of lid morphological features and correlation with other clinical features of MGD can further improve the reliability of objective methods of gland analysis in clinical practice.[25,26] Chen *et al*.[27] in their study on 65-year-old patients, however, inferred that meibography alone is not adequate in the diagnosis of MGD as their study had many asymptomatic patients with dropout changes. This could possibly be explained by the study performed by Kim *et al*.[28] where they described the possibility of compensatory increased secretion by the functional glands, resulting in a lack of symptoms or the presence of a mixed variety of MGD.

Conclusion

In conclusion, in this study, we give normative values for length, width, number of meibomian glands, number of tortuous glands, and drop-out ratio that were computed using our automated software. These can be used in a clinical setting to objectively distinguish between normal and MGD eyes using infrared imaging as a diagnostic tool.

Acknowledgment

Vaitheeshwaran Lalgudi Ganesan for computing interclass correlation coefficient.

Financial support and sponsorship

This work was conducted by Narayana Nethralaya in collaboration with Robert Bosch, Bengaluru. The study did not receive any funding. The prototype was provided by Robert Bosch, Bengaluru.

Conflicts of interest

There are no conflicts of interest.

References

1. Nelson JD, Shimazaki J, Benitez-del-Castillo JM, Craig JP, McCulley JP, Den S, *et al.* The international workshop on meibomian gland dysfunction: Report of the definition and classification subcommittee. Invest Ophthalmol Vis Sci 2011;52:1930-7.
2. Alghamdi YA, Mercado C, McClellan AL, Batawi H, Karp CL, A. Galor A. Epidemiology of meibomian gland dysfunction in an elderly population. Cornea 2016; 35:731-5.
3. Arita R, Itoh K, Inoue K, Kuchiba A, Yamaguchi T, Amano S. Contact lens wear is associated with decrease of meibomian glands. Ophthalmology 2009;116:379-84.
4. Schaumberg DA, Nichols JJ, Papas EB, Tong L, Uchino M, Nichols KK. The international workshop on meibomian gland dysfunction: Report of the subcommittee on the epidemiology of, and associated risk factors for, MGD. Invest Ophthalmol Vis Sci 2011;52:1994-2005.
5. Bron AJ, Tiffany JM. The contribution of meibomian disease to dry eye. Ocul Surf 2004;2:149-65.
6. Nichols KK, Foulks GN, Bron AJ, Glasgow BJ, Dogru M, Tsubota K, *et al.* The international workshop on meibomian gland dysfunction: Executive summary. Invest Ophthalmol Vis Sci 2011;52:1922-9.
7. Arita R, Itoh K, Maeda S, Maeda K, Tomidokoro A, Amano S. Efficacy of diagnostic criteria for the differential diagnosis between obstructive meibomian gland dysfunction and aqueous deficiency dry eye. Jpn J Ophthalmol 2010;54:387-91.
8. Pult H, Nichols JJ. A review of meibography. Optom Vis Sci 2012;89:E760-9.
9. Pult H, Riede-Pult B. Comparison of subjective grading and objective assessment in meibography. Cont Lens Anterior Eye 2013;36:22-7.
10. Arita R, Suehiro J, Haraguchi T, Shirakawa R, Tokoro H, Amano S. Objective image analysis of the meibomian gland area. Br J Ophthalmol 2014; 98:746-55.
11. Finis D, Ackermann P, Pischel N, Konig C, Hayajneh J, Borrelli M, *et al.* Evaluation of meibomian gland dysfunction and local distribution of meibomian gland atrophy by non-contact infrared meibography. Curr Eye Res 2015;40:982-9.
12. Arita R, Itoh K, Inoue K, Amano S. Noncontact infrared meibography to document age-related changes of the meibomian glands in a normal population. Ophthalmology 2008;115:911-5.
13. Arita R, Itoh K, Maeda S, Maeda K, Furuta A, Fukuoka S, *et al.* Proposed diagnostic criteria for obstructive meibomian gland dysfunction. Ophthalmology 2009;116:2058-63e1.
14. Machalinska A, Zakrzewska A, Safranow K, Wiszniewska B, Machalinski B. Risk factors and symptoms of meibomian gland loss in a healthy population. J Ophthalmol 2016;2016:7526120.
15. Llorens-Quintana C, Rico-Del-Viejo L, Syga P, Madrid-Costa D, Iskander DR. A novel automated approach for infrared-based assessment of meibomian gland morphology. Transl Vis Sci Technol 2019; 8:17.
16. Call CB, Wise RJ, Hansen MR, Carter KD, Allen RC. *In vivo* examination of meibomian gland morphology in patients with facial nerve palsy using infrared meibography. Ophthalmic Plast Reconstr Surg 2012;28:396-400.
17. Ibrahim OM, Matsumoto Y, Dogru M, Adan ES, Wakamatsu TH, Shimazaki J, *et al. In vivo* confocal microscopy evaluation of meibomian gland dysfunction in atopic-keratoconjunctivitis patients. Ophthalmology 2012;119:1961-8.
18. Arita R, Itoh K, Maeda S, Maeda K, Furuta A, Tomidokoro A, *et al.* Meibomian gland duct distortion in patients with perennial allergic conjunctivitis. Cornea 2010; 29:858-60.
19. Suzuki T, Morishige N, Arita R, Koh S, Sakimoto T, Shirakawa R, *et al.* Morphological changes in the meibomian glands of patients with phlyctenular keratitis: Amulticenter cross-sectional study. BMC Ophthalmol 2016;16:178.
20. Celik T, Lee HK, Petznick A, Tong L. Bioimage informatics approach to automated meibomian gland analysis in infrared images of meibography. J Optom 2013;6:194-204.
21. Bron AJ, de Paiva CS, Chauhan SK, Bonini S, Gabison EE, Jain S, *et al.* TFOS DEWS II pathophysiology report. Ocul Surf 2017;15:438-510.
22. Knop E, Knop N, Millar T, Obata H, Sullivan DA. The international workshop on meibomian gland dysfunction: Report of the subcommittee on anatomy, physiology, and pathophysiology of the meibomian gland. Invest Ophthalmol Vis Sci 2011;52:1938-78.
23. Pult H, Riede-Pult BH, Nichols JJ. Relation between upper and lower lids' meibomian gland morphology, tear film, and dry eye. Optom Vis Sci 2012;89:E310-5.
24. Ban Y, Shimazaki-Den S, Tsubota K, Shimazaki J. Morphological evaluation of meibomian glands using noncontact infrared meibography. Ocul Surf 2013;11:47-53.
25. Maskin SL, Testa WR. Infrared video meibography of lower lid meibomian glands shows easily distorted glands: Implications for longitudinal assessment of atrophy or growth using lower lid meibography. Cornea 2018;37:1279-86.
26. Crespo-Trevino RR, Salinas-Sanchez AK, Amparo F, Garza-Leon M. Comparative of meibomian gland morphology in patients with evaporative dry eye disease versus non-dry eye disease. Sci Rep 2021;11:20729.
27. Chen X, Badian RA, Hynne H, Tashbayev B, Hove LH, Jensen JL, *et al.* Morphology of meibomian glands in a 65-year-old norwegian population without dry eye disease. J Clin Med 2022; 11:527.
28. Kim HM, Eom Y, Song JS. The relationship between morphology and function of the Meibomian glands. Eye Contact Lens 2018;44:1-5.